Coastal Engineering 115 (2016) 67–78

Contents lists available at ScienceDirect

Coastal Engineering

journal homepage: www.elsevier.com/locate/coastaleng

Empirical wave run-up formula for wave, storm surge and berm width

Hyoungsu Park *, Daniel T. Cox

School of Civil and Construction Engineering, Oregon State University, Corvallis, OR 97331-2302, USA

ARTICLE INFO

Article history:
Received 18 April 2015
Received in revised form 6 October 2015
Accepted 23 October 2015
Available online 30 December 2015

Keywords:
Wave run-up
Iribarren number
Boussinesq model
Hurricane
Dune
Berm

ABSTRACT

An empirical model to predict wave run-up on beaches considering storm wave and surge conditions and berm widths (dry beach) has been derived through a synthetic data set generated from a one-dimensional Boussinesq wave model. The new run-up equation is expressed as a function of a new Iribarren number composed of three regions: the foreshore, the berm or dry beach width, and the dune. The dissipative effect of the berm is included as a reduction factor expressed as a function of the berm width normalized by the offshore wavelength. The equation is relatively simple but is shown to be applicable for a fairly wide variety of berm widths and storm wave conditions associated with extreme events such as hurricanes, and it is shown to be an improvement over existing empirical run-up models that do not consider the berm width explicitly. In addition, the new parameterization of the Iribarren number considering the three regions and the berm width reduction factor are shown to improve other empirical models.

1. Introduction

Many cases of inundation and coastal flooding occur during extreme events such as hurricanes when the maximum wave run-up exceeds the dune crest. Therefore, the severity of hurricanes can be grossly determined by the relation among the wave and surge conditions and the beach morphology (Sallenger, 2000). Although existing time-dependent numerical models provide accurate, deterministic estimates of wave run-up for given boundary conditions, it is nevertheless necessary to develop simplified expressions for wave run-up that can be used, for example, in probabilistic models for a range of surge and wave forcing and morphological conditions. The complex nature of wave run-up on realistic cross-shore profiles prohibits analytical solutions, so simplified run-up formulas rely on empirical approaches based on field observations (e.g., Holman, 1986) and laboratory experiments (e.g., Mase, 1989). Few field observations exist, however, of run-up during extreme storm events (e.g., Senechal et al., 2011), so it is necessary to consider the suitability of these empirical equations for extreme events.

Generally, wave run-up is characterized by the Iribarren number, which is also known as the surf-similarity parameter (Battjes, 1974), and is widely utilized for wave run-up on beaches and coastal structures and for tsunami inundation. The Iribarren number is

$$\xi = \frac{\tan\beta}{\sqrt{H/L}} \tag{1}$$

where β is the angle of the characteristic slope, H is the characteristic wave height, and L is the characteristic wavelength. For consistency, we use the nomenclature "Iribarren number" rather than "surf-similarity parameter" because the parameter is also used for coastal structures and tsunamis without surf zones, and we follow the conventional notation of ξ.

For beaches, β is often taken as the angle of the foreshore slope around the still water shoreline, although other values have been used such as the slope at the breakpoint or the mean slope over the active portion of the surf zone. For coastal structures, β is generally less ambiguous since rubble mound revetments and breakwater are typically built with a constant slope, usually much steeper than sand beaches. The characteristic wave height is typically the deep water wave height, H_0, the wave height at breaking H_b, or, in the case of coastal structures, the incident wave height at the toe of the structure, H_i. Similarly, the characteristic wavelength can be the deep water wavelength $L_0 = gT^2/2\pi$, the wavelength at breaking L_b estimated using linear wave theory and the local water depth at breaking, or the wavelength estimated at the toe of a coastal structure. There are a variety of wave conditions to consider such as regular waves from laboratory studies, irregular waves, and transient waves such as tsunamis. For regular wave studies, H and T are not ambiguous. For the case of irregular waves, H is generally characterized by the

* Corresponding author. Tel.: +1 541 602 8618; fax: +1 541 737 3052.
E-mail addresses: hyoungsu.park@gmail.com (H. Park), dan.cox@oregonstate.edu (D.T. Cox).

http://dx.doi.org/10.1016/j.coastaleng.2015.10.006
0378-3839/

significant wave height H_s, and T is generally characterized by the peak period T_p, although other characterizations are possible such as $H_{1/10}$ or the mean wave period T_m. For transient wave studies such as for tsunamis modeled as solitary waves, H is generally the maximum positive displacement at a given depth, and T is defined as the duration over which the positive displacement exceeds a certain value, for example.

Since Hunt (1959), empirical run-up models have been expressed as a function of the Iribarren number,

$$\frac{R}{H} = K\xi \tag{2}$$

where R is the maximum run-up defined as the vertical projection above the still water level, and K is an empirical constant.

Holman (1986) used field observations of wave run-up at Duck, NC, to develop an empirical run-up model on natural beaches using a similar form as Eq. (2) and is given by

$$\frac{R_{2\%}}{H_0} = 0.83\xi_f + 0.2 \tag{3}$$

where the run-up is the value exceeded by 2% of the run-up events, $R_{2\%}$, normalized by the significant wave height in deep water. The Iribarren number is defined using the angle of the foreshore slope β_f, significant wave height in deep water, and the wavelength in deep water using the peak wave period:

$$\xi_f = \frac{\tan\beta_f}{\sqrt{H_0/L_0}} \tag{4}$$

Mase (1989) developed a similar run-up equation based on irregular waves generated in a laboratory on a plane slopes and is written as

$$\frac{R_{2\%}}{H_0} = 1.86\xi_f^{0.71} \tag{5}$$

where Eq. (4) was used to define the Iribarren number in a similar manner as Holman (1986), and the foreshore slope was the same as the slope for the incident waves prior to breaking and ranged from 1/30 to 1/5.

Using data sets from US East and West Coast beaches, Stockdon et al. (2006) developed an empirical wave run-up model (hereinafter referred to as the "Stockdon model" for brevity) using an Iribarren-like form given as

$$R_{2\%} = 1.1\left(0.35\tan\beta_f(H_0L_0)^{0.5} + 0.5\left[H_0L_0\left(0.563\tan\beta_f{}^2 + 0.0004\right)\right]^{0.5}\right) \tag{6}$$

This model is composed of separate terms to consider different contributions of the wave setup and swash. The swash (the second term on the left hand side of Eq. (6)) is further separated into two parts considering incident wave and infra-gravity wave effects.

In parallel with the development of empirical equations for wave run-up on beaches, there has been significant development for wave run-up equations on coastal structures. Unlike studies on beaches, studies of run-up on coastal structures were developed primarily using laboratory experiments due, in part, to difficulties of direct measurements on coastal structures during storms. Van der Meer and Stam (1992) provided an empirical run-up equation as piecewise continuous function composed of linear and power curve using the Iribarren number

$$\frac{R_{2\%}}{H_s} = \begin{cases} 0.96\xi_m & \xi_m < 1.5 \\ 1.17\xi_m{}^{0.46} & \xi_m \geq 1.5 \end{cases} \tag{7}$$

where ξ_m is the Iribarren number defined using the structure slope, H_s is the significant wave height of the incident waves at the toe of the structure and, and the subscript m denotes that the wavelength is computed using the mean period. This work was later extended by De Waal and Van der Meer (1992) and VanderMeer (1998) to provide a general wave run-up model on dikes to account for the design of the berm, roughness effects of the dike, and wave direction through a combination of reduction factors and is given as

$$\frac{R_{2\%}}{H_s} = 1.6\,\gamma_1\gamma_2\gamma_3\xi_p \tag{8}$$

where the subscript p denotes that Iribarren number is defined using the peak period T_p. The reduction factor γ is a dimensionless number less than 1.0, determined experimentally to account for effects of the berm geometry, γ_1, surface roughness such as natural grass or rock, γ_2, and wave direction, γ_3. This run-up model has an empirical maximum limit of $R_{2\%}/H_s = 3.2\,\gamma_2\,\gamma_3$.

Eqs. (7) and (8) have been widely adopted for the design of coastal structures, and examples of their application are summarized in coastal engineering manuals (e.g., Pullen et al., 2007; USACE, 2003). Similar to run-up models for beaches, some empirical models use slightly different forms of the Iribarren number, particularly when defining the slope because some revetments and dikes may be composed of multiple slopes or may include relatively short, flat berms. The need to account for the profile shape was recognized by Saville (1958), and models generally employ an 'equivalent slope' as summarized by Mase et al. (2013).

Although tsunamis can occur on vastly different scales compared to wind waves on beaches and coastal structures, the Iribarren number has been found to be a suitable parameter for tsunami run-up studies. For example, Kobayashi and Karjadi (1994) combined numerical model results with laboratory experiments to develop an empirical formula to predict the run-up height normalized by the incident solitary wave amplitude (A_0) as a function of Iribarren number, given as

$$\frac{R}{A_0} = 2.955\xi^{0.395} \tag{9}$$

where the Iribarren number is defined using a characteristic period for the solitary wave defined as the duration over which the free surface exceeds $0.05A_0$. Kobayashi and Karjadi (1994) show that Eq. (9) is applicable for $0.125 < \xi < 1.757$ and that changing the definition of the characteristic period based on exceedance of either $0.01A_0$ or $0.1A_0$ changes the predicted run-up on the order of 10%.

The application of Iribarren number for tsunami run-up was analytically studied by Madsen and Fuhrman (2008), and it highlighted that run-up solutions for the canonical run-up depend on Iribarren number for the non-breaking regular wave. Furthermore, Madsen and Schaeffer (2010) provided analytic run-up solutions for the periodic and transient waves in terms of the Iribarren number, considering separate breaking and non-breaking regimes. The solutions are the minimum value between these two terms, given respectively as,

$$\frac{R}{A_0} = \begin{cases} C_1\xi_1^{2.0} \\ C_2\,(A_0/h_0)^{-0.25}\xi_1^{-0.5} \end{cases} \tag{10}$$

where A_0 is the maximum amplitude of the transient (tsunami) wave modeled using a Gaussian profile and h_0 is the water depth offshore and can be idealized as the water depth at the continental shelf. For laboratory studies and numerical simulations, h_0 is typically the water depth in the constant-depth section at the seaward boundary. C_1 and C_2 are analytical constant depending on input wave types (e.g., single wave, $C_1 = 0.1512$ and $C_2 = 4.0513$) as discussed in Madsen and Schaeffer (2010). The Iribarren number ξ_1 is defined by a uniform slope, the amplitude of the single wave A_0, and the deep water wavelength based on a representative period. For the case of a single wave which sustains the solitary wave shape but its frequency is independent

from depth and amplitude, the representative period is the duration of 0.75% of the peak amplitude of the wave.

Park et al. (2015) compared the analytic solutions of Madsen and Schaeffer (2010) with the output of a time-dependent numerical model and found that the run-up in the breaking region was not predicted by Eq. (10), and that the run-up in the non-breaking region was predicted by Eq. (10) only when bottom friction was not included. Park et al. (2015) used data generated by the time-dependent model to modify the solutions of Madsen and Schaeffer (2010) by separating the domain into three regimes (breaking, transition, and non-breaking). Further, Park et al. (2015) defined an offshore and onshore Iribarren number to account for large differences between the bathymetric and topographic slopes, and they also accounted for the effects of bottom friction and breaking numerically which were not possible in the analytical treatment of Madsen and Schaeffer (2010). The empirical model of Park et al. (2015) is expressed as the minimum of three terms for the breaking, transition, and non-breaking regions, respectively, as

$$\frac{R}{A_0} = \begin{cases} 1.2\,\gamma\xi_1^{0.5} \\ 2.5\,\gamma \\ 4.0(A_0/h_0)^{-0.25}\gamma\xi_1^{-0.5} \end{cases} \tag{11}$$

where h_0 is the 100 m water depth, ξ_1 is the offshore Iribarren number defined using the mean slope from the 100 m depth to the shoreline, the amplitude A_0, and the deep water wavelength defined as the duration of a positive wave train exceeding 1% of the maximum amplitude. The empirical constant γ was derived from the numerical simulations and depends on the onshore Iribarren number (ξ_2) and is given as

$$\gamma = [0.9,\ 1.2,\ 1.6] \quad for\ [\xi_2 < 1.8,\ 1.8 \le \xi_2 < 4.5,\ \xi_2 \ge 4.5] \tag{12}$$

where the onshore slope for ξ_2 is defined as the average slope from the still water shoreline to the point of maximum run-up. This equation was applied without recalibration and shown to predict the tsunami run-up for the 2011 Tohoku tsunami reasonably well despite the fact that the model was developed using the output of a one-dimensional numerical model.

This brief introduction highlights that parameterization of run-up using the Iribarren number is successful across a range of scales including wave run-up on beaches, coastal structures, and tsunamis. However, there remain two salient questions for the application for beaches. First, to what extent are existing run-up formulas affected by the presence of the dune–berm system in the case of high surge and waves? Second, in the absence of field observations during extreme conditions, to what extent can the output of time-dependent numerical models be used to improve parameterized wave run-up models to account for the extreme surge and berm?

2. Numerical model setup

2.1. Dune–berm topography and foreshore bathymetry

Fig. 1 shows an example of the idealized cross-shore dune–berm–foreshore profile used for this study where x is the horizontal coordinate positive in the seaward direction with $x = 0$ at the shoreline, and z is the elevation from the still water level ($z = 0$). We developed a simplified dune–berm profile using a berm height (h_B), berm width (W_B), dune height (h_D), and dune width (W_D) based on two assumptions that the berm width is flat and that the dune follows a Gaussian shape. We generated the cross-shore beach profile following the extended equilibrium beach profile of Romańczyk et al. (2005) to avoid the infinite slope at the end of the foreshore slope, specifying the median grain size (D_{50}) and depth of closure (h_C). For simplicity, we prescribed a flat beach profile for $x > 1600$ m and $z < -20$ m since the incident waves are essentially unaffected by the bathymetry for $z < -20$ m.

The dotted line in Fig. 1b shows the observed cross-shore profile at Fire Island, NY, reported by Kraus and Rosati (1997) and is in good agreement with our idealized dune–berm–foreshore profile with $h_B = 2.3$ m, $W_B = 75$ m, $h_D = 3.7$ m, and $W_D = 26$ m. Our idealized profile was examined using four other dune–berm–foreshore systems listed in Table 1 with berm heights and widths ranging $1.6 < h_B < 3.0$ m and $10 < W_B < 75$ m and dune heights and widths ranging $2.6 < h_D < 5.5$ m and $26 < W_D < 100$ m. A dashed line, parallel to the *SWL*, indicates the storm surge level (S) used for the model. S is the overall

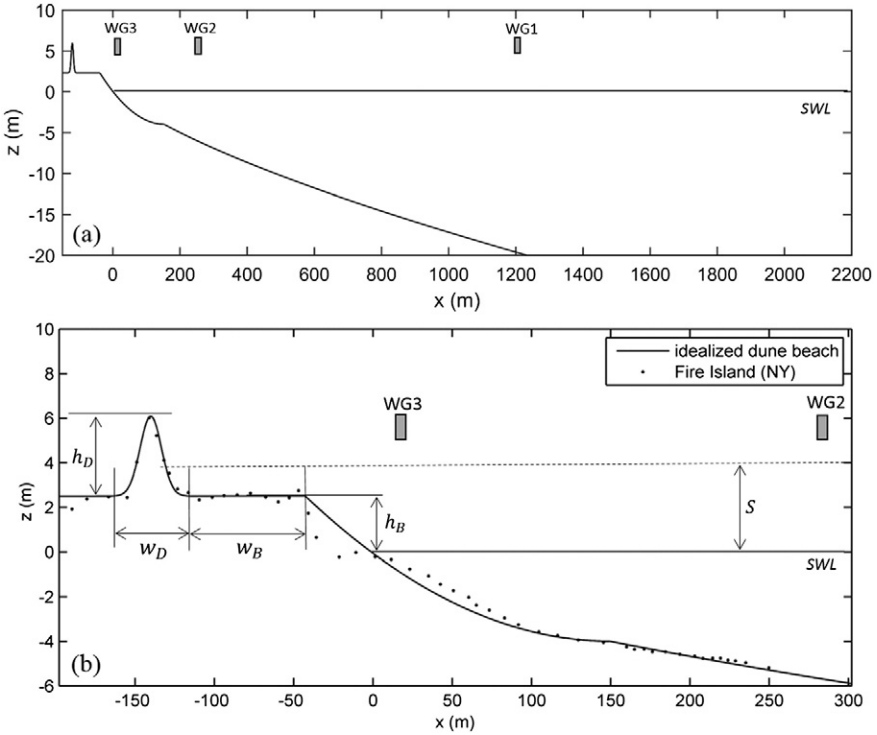

Fig. 1. (a) Idealized cross-shore profile, and (b) and detail of dune–berm–foreshore system. Dotted line shows observed profile at Fire Island, NY (Kraus and Rosati, 1997).

Table 1
Observed dune and berm characteristics.

Location, State	Dune		Berm	
	h_D [m]	W_D [m]	h_B [m]	W_B [m]
Marshfield, MA[(a)]	4.6	100	2.0	35
Fire Island, NY[(b)]	3.7	26	2.3	75
St. John, FL[(c)]	5.0	60	3.0	50
Palm Beach, FL [(c)]	5.5	90	1.6	10
Panama City Beach, FL [(c)]	2.6	70	1.7	40

(a) USACE (1997), (b) Kraus and Rosati (1997), and (c) FDEP (2014).

increased water level due to wind stress, inverse barometric effects, and Coriolis effects associated with wind driven currents. S does not include wave setup effects due to breaking which are captured separately in the numerical model.

2.2. Wave and surge conditions

We considered recent observations of hurricanes in the US to develop realistic surge and wave conditions. On average, there are 6.2 hurricanes per year in the Atlantic Ocean, 1.7 of which make landfall along the US coast (NOAA, 2012). We examined significant wave heights and peak periods during four major hurricanes: Katrina (2005), Gustav (2008), Ike (2008), and Sandy (2012). Considering only buoy data located near the coast ($z > -50$ m), the ranges of observed significant wave heights, H_s and peak periods, T_p were $2 < H_s < 10$ and $10 < T_p < 17$ (Table 2). For simplicity in our model, we defined the storm surge as a uniform and time-invariant increase in water level and applied it for the range of conditions $0 < S < 4.0$ m. Although a much greater range of conditions are possible for storm surge and waves under extreme hurricane events, this represents a reasonable range for input to the model.

2.3. Time-dependent numerical model for synthetic data set

As noted earlier, field observations of wave run-up during extreme wave conditions, including the effects of the dry beach width, are extremely rare. Laboratory studies generally employ plane slopes, and we know of no laboratory studies which used realistic dune–berm–foreshore systems under hurricane wave conditions as described in the previous two sections. Therefore, we employ a time-dependent numerical model to generate a synthetic data set to address our two questions of this study. There are several suitable numerical models based on the nonlinear shallow water wave equations (e.g., Kobayashi et al., 1987; Raubenheimer and Guza, 1996) and Boussinesq equations (e.g., Fuhrman and Madsen, 2008; Kennedy et al., 2000; Madsen et al., 1997). For this study, we used COULWAVE (Lynett et al., 2002) which solves a set of Boussinesq equations with a higher-order finite-volume method because the model is open source and has been validated through a series of bench mark problems for wave run-up and overtopping and for tsunami inundation using both field and laboratory data (Lynett and Liu, 2005; Lynett et al., 2002; Lynett et al., 2003; Park et al., 2013). For wave breaking, COULWAVE applies the eddy viscosity model which is described in Lynett (2006). The model was applied to study the overtopping problem by Lynett et al. (2010). In this study, the complexity of the overtopping over the irregular cross profiles of levees was examined during Hurricane Katrina. Park et al. (2015) developed empirical tsunami run-up equation in a manner similar to that of Kobayashi and Karjadi (1994) as discussed earlier.

Table 2
Observed hurricanes wave conditions to develop range of input conditions.

Hurricane	Year	Category	H_s [m]	T_p or T_m [s]
Katrina[(a)]	2005	5	2–6	10–13
Gustav[(b)]	2008	4	4–5	13–17
Ike[(c)]	2008	4	4–6	10–13[(e)]
Sandy[(d)]	2012	3	5–10	10–15

(a) Wang and Oey (2008), (b) Dietrich et al. (2011), (c) Hope et al. (2013), (d) NDBC (2014), (e) authors reported mean period T_m.

Because the model has been validated extensively already, we use the model 'as is' without changing the parameters for dissipation due to wave breaking. The model uses an adjustable quadratic bottom friction term with a dimensionless friction factor, f, which is typically constant in space and time throughout the simulation. We adjusted the friction factor for the first series of tests as described in the next section, and used the moderate friction value $f = 0.02$ for the remainder of the tests. The model grid size was fixed at 1.0 m for all cases. The run-time of each trial varied from 2500 to 5000 s corresponding to the input wave periods in the range $10 < T_p < 18$ s to assure that we have approximately 250 waves for analysis for each model run. We utilized the TMA spectral shape with default shape parameters (Bouws et al., 1985) and assumed random phases to develop an input irregular wave condition in the model. Three wave gages (WG1, WG2, and WG3) as shown in Fig. 1 were setup at $z = -19.0$, -6.0, and -1.0 m to capture the wave process offshore, in the shoaling region prior to breaking, and in the surf zone after breaking.

2.4. Model cases

Three model cases were tested in this study. Case 1 ($n = 72$ trials) used a range of wave height and periods with no storm surge ($S = 0$) and no effect of the berm height or width. The purpose of Case 1 was to evaluate the overall behavior of the Boussinesq model, including the wave height decay due to breaking and the generation of infra-gravity waves, and to compare the model run-up with conventional empirical equations derived under similar condition. Case 2 ($n = 80$ trials) used a range of wave heights, periods and storm surge levels with a constant berm height and width. The purpose of Case 2 was to understand the influence of the surge level on run-up heights, particularly as the conditions transitioned from wave run-up on the foreshore slope to the dune slope and to evaluate the conventional empirical models under these conditions. Case 3 ($n = 450$ trials) expanded the data set by including a range of berm height and widths and was used to derive a new empirical formula and to make recommendations for improving existing formulas.

Table 3 summarizes the input conditions for Case 1. We created three idealized beach profiles following Romańczyk et al. (2005) as shown in Fig. 1 by specifying three median grain sizes, $D_{50} = 0.3$, 0.4, and 0.5 mm. These values were chosen based on the $D_{50} = 0.4$ mm grain size reported in Hanson et al. (2010) for Long Beach, NY, similar to that shown in Fig. 1. We note that the profile is fixed and cross-shore sediment transport is not considered in this study. Correspondingly, each beach profile had different foreshore slopes in the range $0.023 < \tan\beta_f < 0.091$. The berm height was set as $h_B = 3.5$ m for all three profiles, and we did not include a dune for Case 1. We used moderate wave height conditions ($H_s = 1.0$ and 2.0 m), but we choose relatively long wave periods ($T_p = 10$, 12.5, 15, and 17.5 s). No storm surge levels were included ($S = 0$), thus our berm height was high enough that water did not propagate across the flat berm section. Additionally, we tested three different friction coefficients ($f = 0.01$, 0.02, 0.03) to check the model sensitivity to this parameter.

Table 4 summarizes the input conditions for Case 2. We use only one bathymetry ($D_{50} = 0.3$ mm) with a corresponding foreshore slope of 0.023. We added berm and dune profiles ($h_B = 2.5$ m, $W_B = 55$ m, $h_D = 5$ m, $W_D = 70$ m) similar to that shown in Fig. 1 to test four storm surge levels ($S = 0.0$, 1.0, 2.0, and 3.0 m). Incident wave conditions were more typical of hurricane conditions with wave heights and periods in the range $2.0 < H_s < 5.0$ m and $10 < T_p < 18$ s. The bottom friction remained fixed at $f = 0.02$ for all runs in Case 2.

Table 3
Summary of model input for Case 1.

Case	D_{50} [mm]	$\tan\beta_f$ [−]	H_s [m]	T_p [s]	f [−]	No. of runs
1A	0.3	0.023	1.0, 2.0	10, 12.5, 15, 17.5	0.01, 0.02, 0.03	24
1B	0.4	0.054	1.0, 2.0	10, 12.5, 15, 17.5	0.01, 0.02, 0.03	24
1C	0.5	0.091	1.0, 2.0	10, 12.5, 15, 17.5	0.01, 0.02, 0.03	24

Note: $h_B = 3.5$ m, $S = 0$ m, $W_B = 0$ m, $h_D = 0$ m, $W_D = 0$ m.

Table 5 summarizes the input conditions for Case 3. Similar to Case 2, we used only one bathymetry ($D_{50} = 0.3$ mm) but we had five berm widths ($W_B = 0$, 25, 55, 100, and 200 m). In addition, we simulated surge levels with higher resolution at 0.5 m increments ($S = 1.0$, 1.5, 2.0. 2.5, 3.0, 3.5, and 4.0 m), but slightly lower range of wave height were tested (2.0 *Hs* 4.0 m). Bottom friction was fixed at $f = 0.02$. A total of $n = 450$ cases were simulated in Case 3, and some of Case 3C overlapped with Case 2.

3. Wave run-up results

3.1. Case 1: model behavior, run-up analysis, and existing run-up equations

It is well known that low frequency motions are generated and amplified as waves propagate across the surf and swash zone (Guza and Thornton, 1982) and that these motions play an important role in wave run-up on beaches (Raubenheimer and Guza, 1996; Ruggiero et al., 2001). Therefore, it is necessary to check that the time-dependent model reproduces these phenomena. Fig. 2a–c shows the spectral energy density of surface elevation in the offshore region, at the shoaling region prior to breaking, and in the surf zone, respectively, for Case 1A with $H_s = 2.0$ m, and $T_p = 12.5$ s. The spectra are plotted as a function of normalized frequency, f^*, defined as $f^* = f/f_p$, where f_p is the peak frequency at WG1, so that $f^* = 1$ corresponds to the spectral peak of the incident wave spectrum. Fig. 2a–c shows that the low frequency motion is negligible offshore, increases slightly near breaking, and gives a dominant signal in the surf zone. Similar patterns of wave frequency transformation were reported by many researchers (e.g., Cox et al., 1992; Raubenheimer and Guza, 1996), and time-dependent models have been verified to reproduce the correct wave transformation using laboratory and field data. Therefore, we assume that the time-dependent model correctly reproduces the low frequency motions relevant to the processes of wave run-up.

Friction is one of the free parameters that can be adjusted empirically in the numerical model. Higher values of f induce more dissipation during wave propagation and swash run-up, and therefore decrease the run-up. Based on the assumption that the Stockdon model can predict the wave run-up data on the natural beach idealized in Case 1, we compared the Stockdon model with the numerical model results to calibrate the bottom friction as discussed later.

Fig. 3a shows the time-series of the run-up over the entire time series for the same example run shown in Fig. 2, and Fig. 3b shows a detail of the run-up for $1400 < t < 1850$ s. The stars in Fig. 3b are used to indicate the individual run-up maxima. The overall characteristics of the run-up shown in Fig. 3b are similar to that for field and laboratory studies, and the total number of run-up maxima for a given run is significantly lower than the number of incident waves owing to surf and swash zone processes such as bore-capture and run-up/rundown collisions simulated in the time-dependent model. For example, the number of incident waves was 230, but the total number of run-up maxima was 163 for the case of Fig. 3.

Fig. 4 shows the cumulative probability density function of the run-up where each individual run-up event (marked by a star in Fig. 3b, for example) is plotted as a dot in Fig. 4. Due to the discretization of the model with approximately 0.11 m spacing, the run-up events appear in discrete bins along the x-axis. The solid curve is an interpolation through the mean value of each bin. We use this interpolated curve to estimate the following run-up statistics: $R_{\max}$, defined as the maximum run-up height among the individual events; $R_{2\%}$ defined as the average of the highest 2% run-up events; $R_{1/10}$, the average of highest 1/10 run-up events; and $R_{1/3}$, the average of the highest 1/3 run-up events. Of these statistics, we use $R_{2\%}$ as the representative run-up value for this study to be consistent with earlier studies of extreme run-up on beaches (e.g., Holman, 1986; Mase, 1989; Ruggiero et al., 2001; Stockdon et al., 2006) and structures (Pullen et al., 2007; Van der Meer and Stam, 1992; VanderMeer, 1998).

Fig. 5 compares the numerical data from Case 1 (symbols) with predictions of the empirical model by the Stockdon model (lines). Case 1A (circle), 1B (triangle), and 1C (diamond) show the different foreshore slope condition from mild to steep, and the solid, dash, and dash-dot line show the corresponding Stockdon model results. Both the numerical data and the Stockdon model show that $R_{2\%}$ increases linearly with increasing $(H_0L_0)^{0.5}$. The numerical data were generated using a bottom friction $f = 0.02$. Comparisons of the data with the Stockdon model for the two other values of bottom friction (0.01, 0.03) gave less satisfactory agreement, so $f = 0.02$ was adopted for the remainder of this study. This value is reasonable compared to other numerical studies of wave run-up on beaches (e.g., Chen et al., 2000; Liu and Cho, 1994; Lynett, et al., 2002).

Fig. 6 shows Case 1 model results (symbols, same notation as Fig. 5), with the run-up normalized by the significant offshore wave height ($R_{2\%}/H_0$) plotted as a function of the Iribarren number based on the foreshore slope, ξ_f, in Eq. (4). The data for the three different slopes collapse onto nearly a single curve, highlighting the utility of this parameter over the dimensional form $(H_0L_0)^{0.5}$. We note that there is still some scatter, due to the nature of using $R_{2\%}$ based on the average of approximately four individual run-up events per run, and plots of R_s/H_0 vs. ξ_f and R_{ave}/H_0 vs. ξ_f showed considerably less scatter. The empirical model of Holman (1986) shown by the dash line (Eq. (3)) and based on field observations underestimates the normalized run-up, and the model of Mase (1989) based on laboratory observations over a plane slope overestimates the run-up. Nevertheless, we use the general form of these equations (without the y-intercept for simplicity) fitted to the numerical data as a function of ξ_f

$$\frac{R_{2\%}}{H_0} = 1.35\xi_f^{\,0.65} \tag{13}$$

and use this as a baseline when comparing with the more complicated cases including storm surge and berm width.

Table 4
Summary of model input for Case 2.

Model case	S [m]	H_s [m]	T_p [s]	No. of runs
2A	0.0	2.0, 3.0, 4.0, 5.0	10, 12, 14, 16, 18	20
2B	1.0	2.0, 3.0, 4.0, 5.0	10, 12, 14, 16, 18	20
2C	2.0	2.0, 3.0, 4.0, 5.0	10, 12, 14, 16, 18	20
2D	3.0	2.0, 3.0, 4.0, 5.0	10, 12, 14, 16, 18	20

Note: $D_{50} = 0.3$ mm, $h_B = 2.5$ m, $W_B = 55$ m, $h_D = 5$ m, $W_D = 70$ m.

Table 5
Summary of model input for Case 3.

Model case	W_B [m]	S [m]	H_s [m]	T_p [s]	No. of runs
3A	0	1.0, 1.5, 2.0, 2.5, 3.0, 4.0	2.0, 3.0, 4.0	10, 12, 14, 16, 18	90
3B	25	1.0, 1.5, 2.0, 2.5, 3.0, 4.0	2.0, 3.0, 4.0	10, 12, 14, 16, 18	90
3C	55	1.0, 1.5, 2.0, 2.5, 3.0, 4.0	2.0, 3.0, 4.0	10, 12, 14, 16, 18	90
3D	100	1.0, 1.5, 2.0, 2.5, 3.0, 4.0	2.0, 3.0, 4.0	10, 12, 14, 16, 18	90
3E	200	1.0, 1.5, 2.0, 2.5, 3.0, 4.0	2.0, 3.0, 4.0	10, 12, 14, 16, 18	90

Note: $D_{50} = 0.3$ mm, $h_B = 2.5$ m, $h_D = 5$ m, $W_D = 70$ m.

3.2. Case 2: run-up with varying surge levels

For Case 2, we add a dune–berm profile following the idealized cross-shore profile shown in Fig. 1 with $h_B = 2.5$ m, $W_B = 55$ m, $h_D = 5$ m, $W_D = 70$ m, and $\tan\beta_f = 0.023$ and apply four storm surge levels ($S = 0.0$, 1.0, 2.0, and 3.0 m). In Fig. 7, the numerical data show that, for a given value of $(H_0L_0)^{0.5}$, the run-up is nearly the same for the first two cases ($S = 0.0$ and 1.0 m). For $S = 2.0$ m, the run-up is in a transition from being foreshore dominant to being dune dominant and there is no clear trend. However, as the surge level increases to $S = 3.0$ m, the run-up is significantly higher because the run-up is dominated by the dune slope at this level. Fig. 7 also compares these numerical data to the Stockdon model where the solid line is Eq. (6) using the foreshore slope ($\tan\beta_f = 0.023$) and the dashed line uses the dune slope ($\tan\beta_D = 0.143$) defined as a dune steepness ($2h_D/W_D$) for simplicity in this study. As expected from the comparison shown in Fig. 5, the Stockdon model agrees with the numerical data when the surge level is low and the run-up is confined to the foreshore slope. However, the Stockdon model significantly underpredicts the run-up when the surge level is high ($S = 3.0$ m, square symbols). Alternatively, the dashed line shows that the Stockdon model overpredicts all of the numerical data when the dune slope is used. This is likely due to the 55 m wide dune used for this portion of the study which causes additional wave dissipation.

Fig. 8 shows the data of Fig. 7 replotted as the normalized run-up $R_{2\%}/H_0$ versus the Iribarren number based on foreshore slope ξ_f. Not surprisingly for the cases where the surge level was low and the dry beach width was not a major factor, the model of Holman (dashed) provides a lower bound estimate, the model of Mase (dash-dot) provides an upper bound, and the calibrated model (Eq. (13)) provides a reasonable estimate. All of these models underpredict the highest surge case (square symbols). In summary, Figs. 7 and 8 highlight the shortcomings of existing empirical models to predict extreme run-up with elevated surge over some fixed width of dry beach similar to that shown in Fig. 1.

3.3. Case 3: considering a range of berm widths and surge levels

In Case 3 we consider a wide range of berm widths and surge levels to develop a better understanding of how berm width affects wave run-up. Fig. 9 shows the numerical run-up data with circles shaded from black to white for Case 3A ($W_B = 0$ m), 3B ($W_B = 20$ m), 3C ($W_B = 55$ m), 3D ($W_B = 100$ m), and 3E ($W_B = 200$ m). Although there is

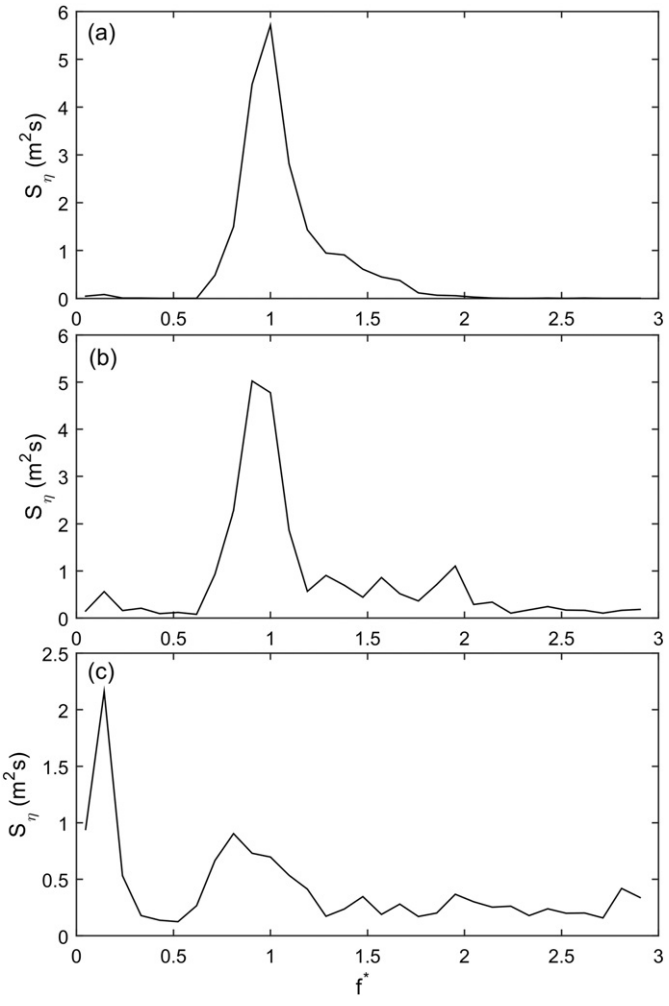

Fig. 2. Spectral densities of surface elevation for Case 1A as a function of normalized frequency, f^* at (a) WG1 offshore, (b) WG2 in the shoaling region, and (c) WG3 in the surf zone.

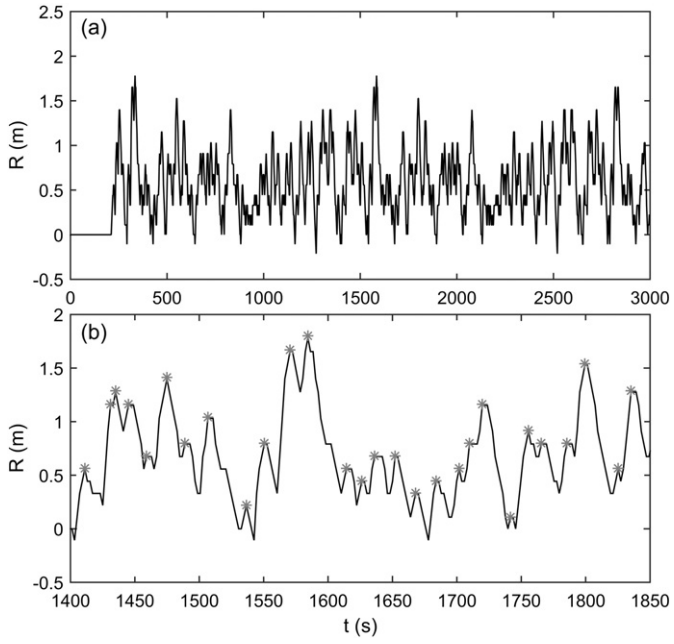

Fig. 3. (a) Run-up for Case 1A, and (b) detail of upper panel. Star symbol indicates local run-up maximum.

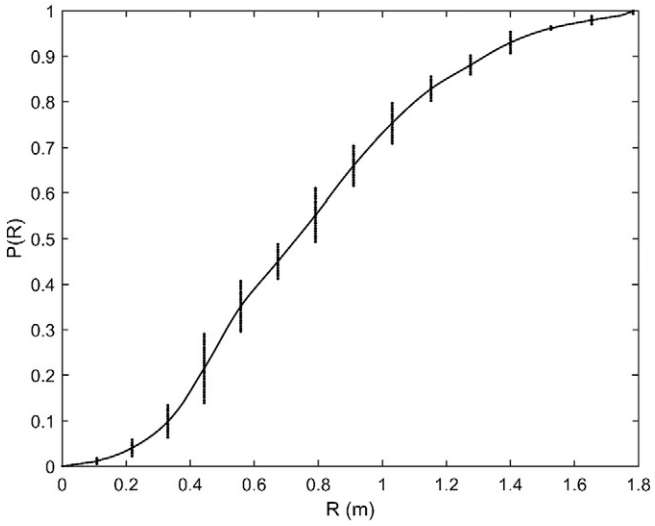

Fig. 4. Cumulative probability density of wave run-up for Case 1A. Individual run-up events (star symbols in Fig. 3) are plotted as discrete dots and appear as vertical lines in discrete bins. Solid curve is interpolation through the mean of each cluster of dots.

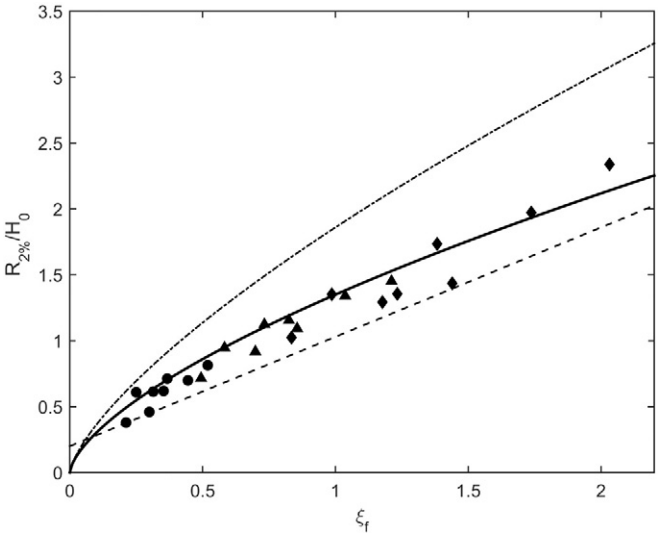

Fig. 6. Comparisons of normalized run-up among the numerical model for Case 1A (circle), 1B (triangle), and 1C (diamond) and models of Holman (dashed), Mase (dash-dot), and Eq. (13) (solid).

significant scatter in these data, there is a general trend of a decrease in run-up as the berm width increases. The Stockdon model is shown using the foreshore (solid) and dune (dash) slopes as in Fig. 7. Fig. 9 shows that the Stockdon model based on the dune slope no longer provides an upper bound to the run-up as several of the run-up values for Case 3A with $W_B = 0$ m exceed the Stockdon model predictions. Similarly, the Stockdon model no longer provides a lower bound based on the foreshore slope, particularly for Case 3E with berm width of 200 m, noting that it is likely that this condition is beyond the range for which the model was calibrated and less likely to occur on natural beach.

4. New empirical run-up equation

In this section, we developed new run-up equations based on the modeling experience provided by Cases 1 to 3 and on the comparisons with existing empirical formulas. The range of Iribarren number used in Case 1 and Case 3 is only validated for the breaking wave run-up condition ($\xi_f < 2$). In developing this new equation, we kept the general form of Eq. (13) where the run-up is normalized by the significant offshore wave height ($R_{2\%}/H_0$) and expressed as a function of the Iribarren number. We found it is useful to redefine the Iribarren number based on the foreshore–dune region as explained in Section 4.1 and to introduce a dimensionless reduction factor to account for berm width, similar to the reduction factors used in run-up on coastal structures to account for energy loss due to porous armor stones as explained in Section 4.2.

4.1. Run-up Iribarren number

We consider the cross-shore to be composed of three regions: (1) the foreshore slope dominant region where the swash occurs only on the beach slope and does not interact with the berm, (2) a transition slope dominant region where the swash occurs at both the foreshore slope and the dune slope regions, and (3) the dune slope dominant region where the swash only occurs at the dune slope. To reflect those three regions, we introduce a new Iribarren number for run-up, ξ_R composed of three parameters ξ_f, ξ_T, and ξ_D where the subscripts f, T, and D

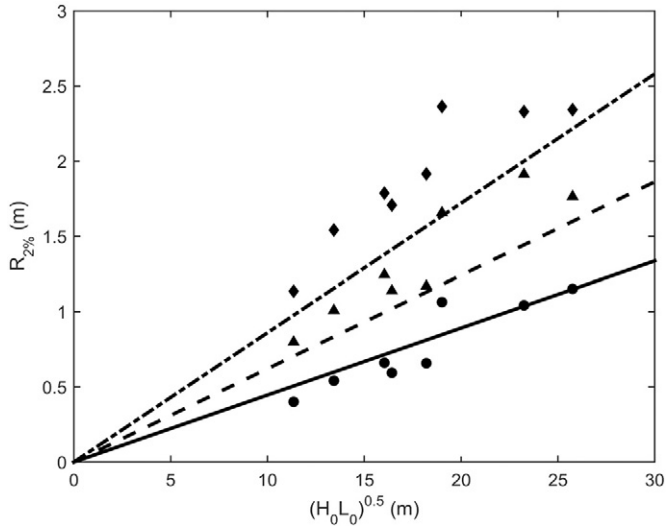

Fig. 5. Run-up comparisons between the numerical model (circle, triangle, and diamond) and the Stockdon model (solid, dash, and dash-dot) for Case 1A, 1B, and 1C, respectively.

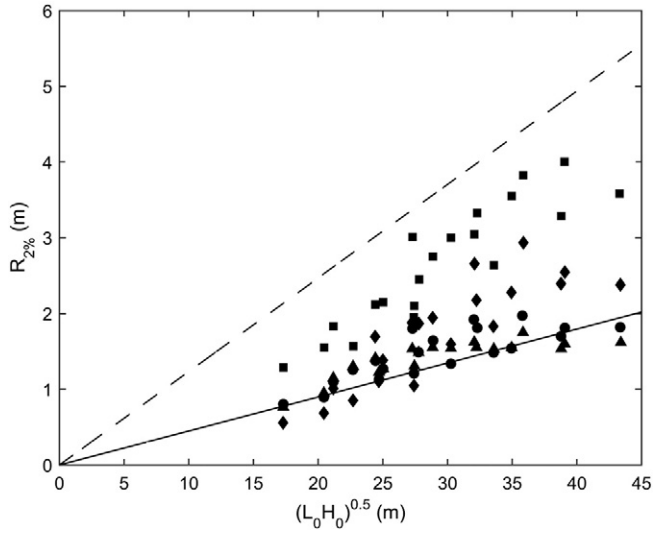

Fig. 7. Run-up for Case 2 considering a range of surge levels. Symbols show numerical model data for $S = 0.0$ m (circle), 1.0 m (triangle), 2.0 m (diamond), and 3.0 m (square), and the Stockdon model uses foreshore slope (solid) and dune slope (dash).

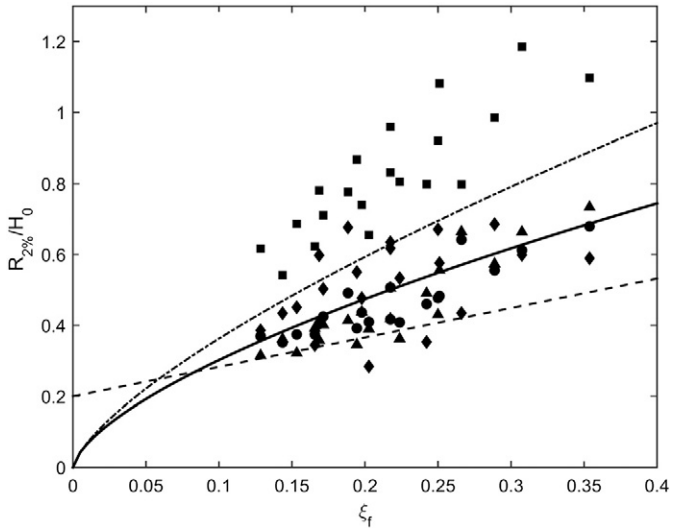

Fig. 8. Normalized run-up for Case 2 considering a range of surge levels. Symbols are the same as Fig. 7, and lines are for models of Holman (dash), Mase (dash-dot), and Eq. (13) (solid).

represent foreshore, transition and dune slope dominant regions, respectively. The boundary of each region depends on the berm height, storm surge level, and deep water wave height and was determined empirically as follows. First, we assume that if the sum of the storm surge level and 70% of the deep water wave height is less than berm height, then there is no significant wave action over the berm, and the run-up swash is limited primarily to the foreshore slope dominant region. The representative slope angle for this region is β_f, and the corresponding Iribarren number is ξ_f. Second, if the storm surge level is greater than the sum of the berm height and 70% of the deep water wave height (Eq. (14)), then we assume that swash motion occurs only on the dune slope due to the high surge level and is not impacted by the foreshore slope (Eq. (15)). Thus, the representative slope is dune slope, β_D, and the corresponding Iribarren number is ξ_D. Last, the region between the foreshore slope and dune slope dominant region is defined as a transition slope dominant region where β_T is used to represent a fictitious transition slope which is a combination of both the foreshore slope and dune slope (Eq. (16)). The corresponding Iribarren number is denoted ξ_T. Summarizing these definitions, we have

$$\xi_f = \frac{\tan\beta_f}{\sqrt{H_0/L_0}}, \qquad for \qquad h_B - S \le 0.7H_0 \tag{14}$$

$$\xi_D = \frac{\tan\beta_D}{\sqrt{H_0/L_0}}, \qquad for \qquad S - h_B \ge 0.7H_0 \tag{15}$$

$$\xi_T = \frac{\tan\beta_T}{\sqrt{H_0/L_0}}, \qquad for \qquad -0.7H_0 < S - h_B < 0.7H_0 \tag{16}$$

For simplicity, we assume that the transition slope β_T varies linearly from foreshore to dune slope as the storm surge level changes and is given as

$$\beta_T = (1-\alpha)\beta_f + \alpha\beta_D \tag{17}$$

where α increases linearly 0 to 1 as a function of storm surge level, berm height, and wave height and was found empirically to be

$$\alpha = \frac{(S - h_B) + 0.7H_0}{1.4H_0} \quad , Min\ [\alpha] = 0\ \&\ \text{Max}\ [\alpha] = 1 \tag{18}$$

where *Min* and *Max* are the minimum and maximum value, and α ranges between 0 and 1. Eq. (18) provides a continuous function since $\alpha = 0$ at the lowest boundary of the transition region where $S\text{-}h_B = -0.7\,H_0$, so that $\beta_T = \beta_f$. Conversely, $\alpha = 1$ at the highest boundary of the transition region where $S\text{-}h_B = 0.7\,H_0$, and $\beta_T = \beta_D$.

To test the validity of Eqs. (14)–(18), we use Eq. (13) which was calibrated for Case 1, and replace ξ_f with ξ_R. Fig. 10 shows the run-up data from Case 1 and Case 3 plotted against the run-up Iribarren number, ξ_R, where the shaded symbols are same as Fig. 9 to identify the changes in berm width and the three regions are differentiated as the foreshore slope dominant region (square), transition slope dominant region (triangle), and dune slope dominant region (circle). The solid line presents our fitted curve results applying ξ_R to Eq. (13) and works well for the foreshore slope dominant regions (square) and, not surprisingly, provides only an upper bound to the rest of the data (triangle, circle) and does not account for the effects of berm width.

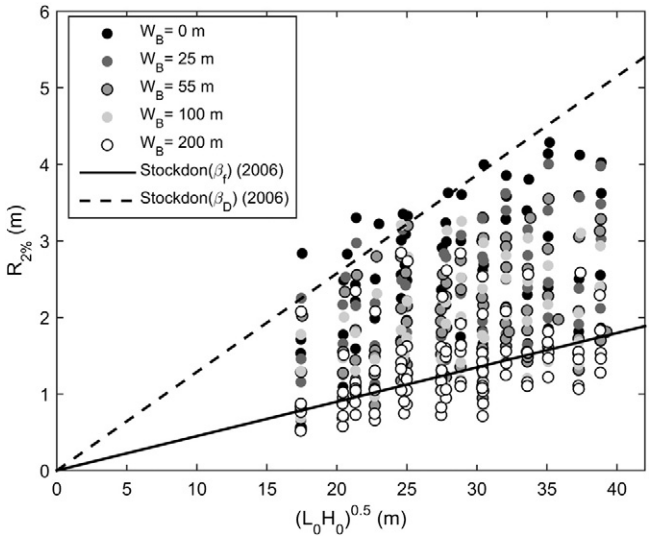

Fig. 9. Run-up for Case 3 with the range of surge and berm widths and the Stockdon model using foreshore (solid) and dune (dash) slopes.

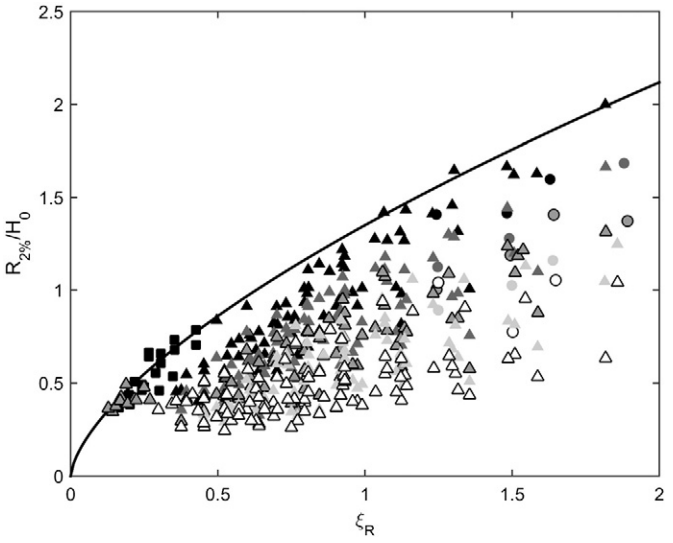

Fig. 10. Normalized run-up for Case 1 and Case 3 as a function of ξ_R and differentiated as a foreshore (square), transition (triangle) and dune (circle) slope dominant region. Shading to differentiate berm width is the same as Fig. 9. Solid line shows Eq. (13) with ξ_R.

4.2. Parameterization of berm width

To incorporate the effect of berm width, we introduce a constant '*C*' as a reduction factor, conceptually similar to that used by De Waal and Van der Meer (1992) for coastal structures. Our new run-up equation for foreshore-transition-dune slope beach condition is

$$\frac{R_{2\%}}{H_0} = 1.35C\xi_R^{0.65} \tag{19}$$

where *C* is the reduction coefficient expecting that *C* is near 1 when the berm width is small and decreases as the berm width increases, and ξ_R chosen among ξ_f, ξ_T, and ξ_D defined by Eqs. (14)–(16), depending on the geometric conditions of H_0, *S*, and *h*. To parameterize *C* based on berm width and to keep the system of equation dimensionless, we use the offshore wavelength L_0 as a scaling parameter so that the dimensionless berm width is $W_B^* = W_B/L_0$ and the functional form is determined empirically from the synthetic data.

Fig. 11 shows the numerical run-up data for Case 1 and 3 as a function W_B^*. To develop a suitable curve through these data, we considered the data in bins and computed the mean value (circle) and a more conserve value based on average of all values exceeding the mean for a given bin (triangle). Two curves were fit through the mean and conservative values, and are given by

$$C = 0.8 - 0.4\tanh(2.0w_B^*) \tag{20}$$

$$C = 1.0 - 0.5\tanh(2.0w_B^*) \tag{21}$$

Both mean and conservative curves show that *C* decreases significantly for $W_B^* < 0.5$, *and decreases more gradually for* $W_B^* > 1.0$ *implying that there can be a significant reduction in wave run-up when the berm (dry beach) width is extended from* $W_B = 0$ *to* $W_B = L_0/2$. *However, Fig. 11 implies there is relatively little benefit in extending the dry beach width beyond one wavelength for reducing wave run-up for this idealized case that does not consider morphological changes. In any case, the reduction factor C reaches a lower limit of 0.5 (conservative) or 0.4 (mean), similar to the work of VanderMeer (1998) for coastal structures.*

Fig. 12a–e shows the normalized run-up plotted as a function of ξ_R for the five berm conditions, W_B = 0, 25, 55, 100, and 200 m. For reference, the solid line is Eq. (19) ignoring the effect of the berm width ($C = 1$). The dashed and dash-dot lines include the berm effect

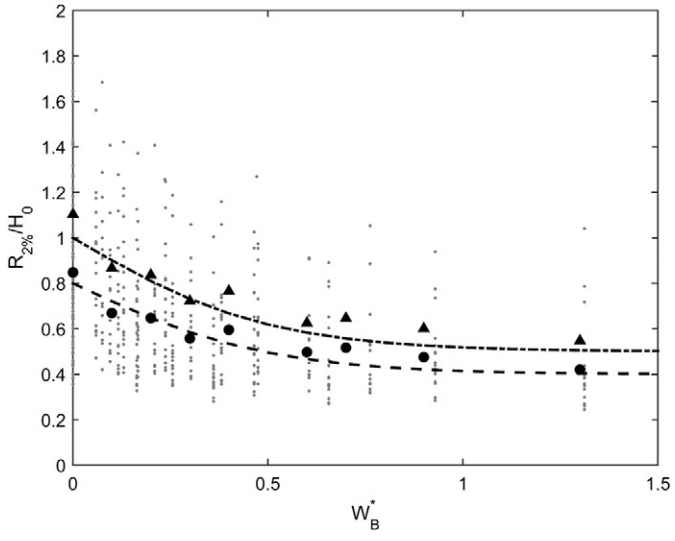

Fig. 11. Dimensionless run-up (dots) as a function of a normalized berm width (W_B^*). *Mean value (circle) and average of values exceeding the mean (triangle). Curves fitted through large symbols given by Eq. (20) (dash) and Eq. (21) (dash-dot).*

with *C* modeled using the average values (Eq. (20)) and are plotted using constant values of T_p = 18 s and T_p = 10 s, respectively, to cover the range of wave periods used to produce the data in each panel. These two lines collapse to a single curve when $W_B = 0$ (Fig. 12a) and are lower than the solid curve because we are using the less conservative Eq. (20) for illustration. In summary, Fig. 12 shows that the functional form of Eq. (19) with the new run-up Iribarren number ξ_R and the berm reduction factor based on the berm width normalized by the deep water wavelength (Eq. (20)) behaves reasonably well to incorporate storm surge and berm effects.

Finally in this section, we note that the original Stockdon model (Eq. (6)) can be modified using the ideas developed herein. We propose the modified Stockdon model, version 1, as

$$R_{2\%} = 1.1\left(0.35\tan\beta_R(H_0L_0)^{0.5} + 0.5\left[H_0L_0\left(0.563\tan\beta_R{}^2 + 0.0004\right)\right]^{0.5}\right) \tag{22}$$

where the foreshore slope, β_f of the original equation (Eq. (6)) is replaced by a run-up slope, β_R which represents three slope conditions, β_f, β_T, and β_D depending on the surge level (*S*), berm height (h_B), and wave height (H_0) as given by Eqs. (17) and (18). Also, we propose the modified Stockdon model, version 2 as

$$R_{2\%} = 1.1C\left(0.35\tan\beta_R(H_0L_0)^{0.5} + 0.5\left[H_0L_0\left(0.563\tan\beta_R{}^2 + 0.0004\right)\right]^{0.5}\right) \tag{23}$$

which adapts the berm width reduction factor, *C*.

Fig. 13 shows four comparisons of the normalized numerical run-up data from Case 1 and Case 3 versus the run-up predictions from (a) the new model using Eq. (20) for reduction factor, (b) the original Stockdon model (Eq. (6)), (c) the modified Stockdon model, version 1 (Eq. (22)) and (d) the modified Stockdon model, version 2 (Eq. (23)) using Eq. (21) for reduction factor. Perfect agreement is shown by the solid line, and the corresponding values of the correlation (ρ^2), root-mean-square error (*RMSE*) and bias are listed in Table 6 along with values from comparison to the original models of Holman (1986) and Mase (1989).

Fig. 13a shows that the new model gives satisfactory agreement when compared to the data for which it was calibrated and gives the highest correlation coefficient and lowest *RMSE*. The original Stockdon model has a negative correlation and large *RMSE*, indicating that it would provide poor prediction of run-up for the idealized profile shown in Fig. 1 over the range of conditions listed in Table 5. Detailed inspection of the model-data comparison showed that the largest deviation was due to the berm effects not originally included in the Stockdon model. Fig. 13c in which only our run-up slope parameterization (β_R) is adopted, shows that the first modification to the Stockdon model slightly overpredicts the run-up (bias = 0.090 m) and provides improvement to the original equation ($\rho^2 = 0.42$). Fig. 13d in which both our run-up slope parameterization and berm width reduction are adopted, shows that the Stockdon model has the correlation and *RMSE* a little bit lower than the new model.

5. Discussion

In this section we acknowledge some of the limitations of our proposed model, discuss the comparisons with the original Stockdon model, and offer some suggestions for improvement.

First, our model was developed using synthetic data under fairly idealized cross-shore profile conditions. Although we constructed the morphology using observed profiles (Table 1), based the surge and wave forcing conditions on a range of observed conditions (Table 2), and used a time-dependent numerical model to simulate the relevant nearshore processes of breaking, amplification of low frequencies, and

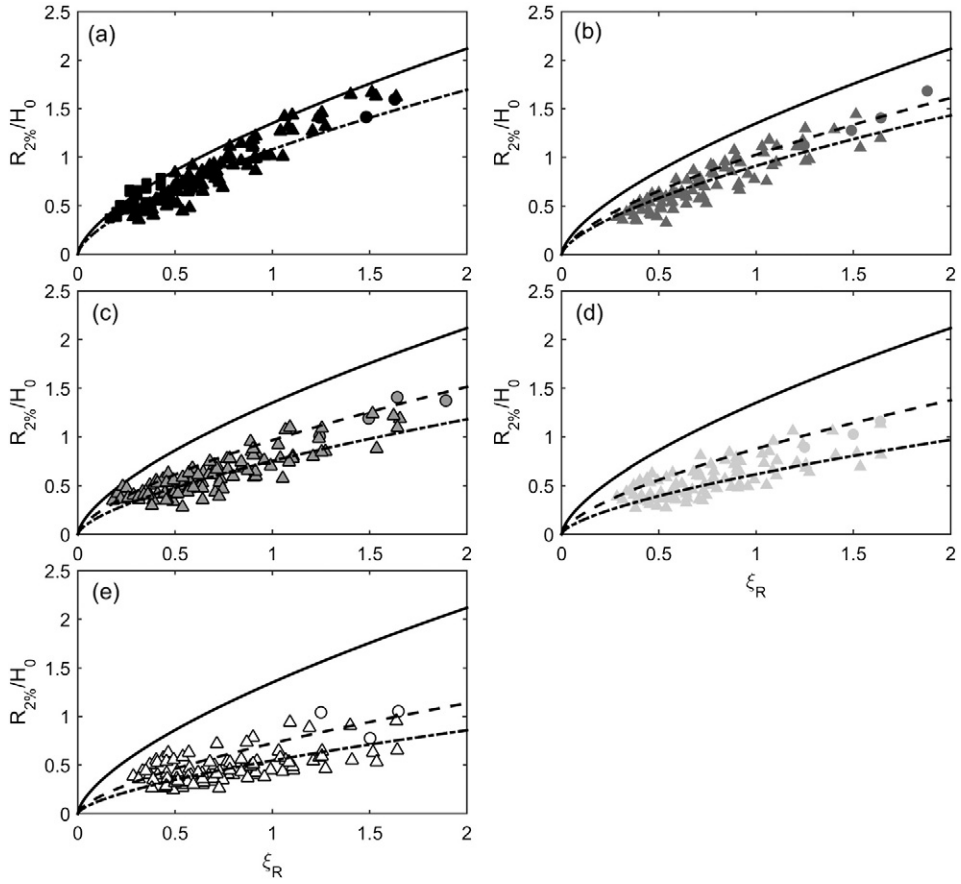

Fig. 12. Normalized run-up as a function of a run-up Iribarren number (ξ_R) from Case 3 for the six berm widths (a) $W_B = 0$, (b) 25, (c) 55, (d) 100, and (e) 200 m. Eq. (19) with $C = 1$ (solid), Eq. (20) for $T_p = 18$ s (dash) and $T_p = 10$ s (dash-dot).

swash (Figs. 2 and 3), there are limitations to this approach. For example, there is no morphological response in our model, and it is well known that the nearshore morphology responds quickly (on the scale of hours), so that relevant parameters such as foreshore slope and berm width are not constant during large storms. There is no variation in surface roughness in our model. In nature, there is often vegetation or other ecological influences that may change the surface roughness and, therefore, it changes the run-up, particularly over the berm and dune regions impacted by waves and surge only during extreme events. Similarly, we do not include percolation into the sand that may alter the run-up statistics. We limited our analysis to the cross-shore only and included no effects of wave direction. For steep coastal structures, this is particularly important because waves will undergo less refraction. On milder beaches, we anticipate that the waves are generally shore-normal during run-up due to refraction, so we anticipate that wave direction may be less important compared to morphological changes, surface roughness, and percolation.

Second, our model has been developed and 'verified' using the same data set. In the future, it will be necessary to use an independent source for model verification through field observations and laboratory testing. We acknowledge that the comparison of our model and the Stockdon model in Figs. 13a and b is limited in some sense because our model was calibrated using the same data for which the comparisons were made and the Stockdon model was calibrated using another data set. On the other hand, the Stockdon model does not include the effects of the berm width explicitly, so it would be unlikely that recalibration of the original Stockdon model to the numerical data would offer much improvement. Third, we show that the Stockdon model can be improved significantly by adopting a new definition of the run-up slope (β_R) and by adopting a reduction factor (C) to account for the berm width. On the other hand, we found that the format of our new equation is simpler and consistent with earlier studies of run-up on beaches, coastal structures and tsunamis. Consistent with these earlier studies, the form of our equation is dimensionless, including the parameterization of the berm width reduction factor. Moreover, the effects of surface roughness, percolation, and other energy losses can easily be incorporated through a series of reduction coefficients, similar to the work of VanderMeer (1998) for coastal structures.

6. Conclusion

This study highlights the role of the berm width in affecting wave run-up during extreme surge events and the limitations of existing empirical approaches to predict run-up in these conditions. Using a synthetic data set derived from a time-dependent Boussinesq wave model over an idealized cross-shore profile, we develop a new run-up model using a new run-up Iribarren number to account for the dune, transition and foreshore dominant regions and utilize a new berm reduction factor parameterized using the berm geometry and offshore wavelength. The main conclusions of this work are:

1. Under conditions of hurricane storm surge and waves, the existence of a berm is shown to influence the wave run-up, primarily through dissipation of wave energy across the berm (Fig. 12).
2. The empirical wave run-up models of Holman (1986), Mase (1989) and Stockdon et al. (2006) did not compare well with the synthetic data set when the cross-shore profile included a wide berm and a storm surge and waves of typical hurricane conditions (Fig. 13b, Table 6).
3. The Iribarren number (Eq. (8)) is adequate foam to describe the run-up on beaches with berms under hurricane surge and wave conditions when the Iribarren number is modified to account for the

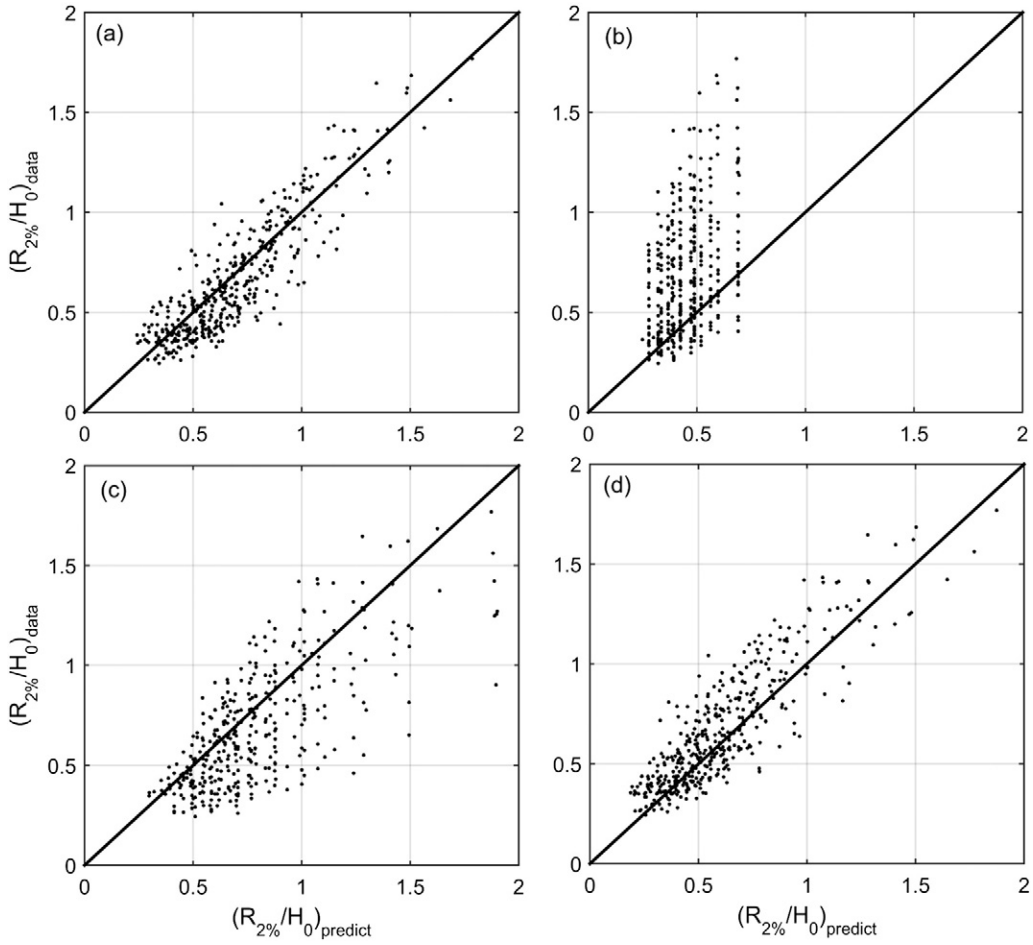

Fig. 13. Comparisons of numerical data with predictions by (a) new equation (Eq. (19)), (b) original Stockdon model (Eq. (6)), (c) modified Stockdon model v1 (Eq. (22)), and (d) modified Stockdon model v2 (Eq. (23)).

dune, transition and foreshore regions and when the influence of the berm is included as a reduction factor for the idealized conditions used to generate the data in this paper (Fig. 13a, Table 6).

4. The existing model of Stockdon et al. (2006) can be improved for predicting run-up under hurricane surge and wave conditions and for coastal berms and dunes by adopting the run-up Iribarren number and berm reduction factor described in this paper (Fig. 13d, Table 6).

This study is based on a synthetic data set, and although the model used to generate the data has been validated over a wide range of nearshore conditions, there are several model simplifications – particularly the lack of a moveable bed – which should be taken into account. Therefore, the new model requires verification through field observations and laboratory testing under hurricane surge and wave condition. In addition, further research is necessary to incorporate effects of coastal vegetation, percolation, and wave direction.

Table 6
Correlation coefficient, *RMSE*, and bias for model-data comparisons.

Model	ρ^2	*RMSE* [m]	Bias [m]
New model	0.74	0.135	0.028
Stockdon	−8.26	0.339	−0.208
Stockdon, v1	0.42	0.227	0.090
Stockdon, v2	0.67	0.154	−0.061
Holman	−91.86	0.576	−0.505
Mase	−17.55	0.485	−0.400

Acknowledgment

This research is based upon work partially supported by the National Science Foundation under Grant No. 1356978. Any opinion, findings, and conclusions or recommendations expressed in this document are those of the authors and do not necessarily reflect the views of the National Science Foundation. The authors thank three anonymous reviewers for their constructive comments.

Appendix A. Supplementary data

Supplementary data to this article can be found online at http://dx.doi.org/10.1016/j.coastaleng.2015.10.006.

References

Battjes, J.A., 1974. Surf similarity. Coast. Eng. Proc. 1 (14), 466–480.
Bouws, E., Gunther, H., Rosenthal, W., Vincent, C., 1985. Similarity of the wind wave spectrum in finite depth water: 1. Spectral form. J. Geophys. Res. Oceans 90 (C1), 975–986 (1978–2012).
Chen, Q., Kirby, J.T., Dalrymple, R.A., Kennedy, A.B., Chawla, A., 2000. Boussinesq modeling of wave transformation, breaking, and runup. II: 2D. J. Waterw. Port Coast. Ocean Eng. 126 (1), 48–56.
Cox, D.T., Kobayashi, N., Wurjanto, A., 1992. Irregular wave transformation processes in surf and swash zones. Coast. Eng. Proc. 1 (23), 156–169.
De Waal, J.P., Van der Meer, J.W., 1992. Wave run-up and overtopping on coastal structures. Coast. Eng. Proc. 1 (23), 1758–1774.
Dietrich, J.C., Westerink, J.J., Kennedy, A.B., Smith, J.M., Jensen, R.E., Zijlema, M., et al., 2011. Hurricane Gustav (2008) waves and storm surge: hindcast, synoptic analysis, and validation in southern Louisiana. Mon. Weather Rev. 139 (8), 2488–2522.

FDEP, 2014. Florida Department of Environmental Protection, Historical Shoreline Database. http://www.dep.state.fl.us/beaches/data/his-shore.htm (Accessed 09/25/2014.).
Fuhrman, D.R., Madsen, P.A., 2008. Simulation of nonlinear wave run-up with a high-order Boussinesq model. Coast. Eng. 55 (2), 139–154.
Guza, R.T., Thornton, E.B., 1982. Swash oscillations on a natural beach. J. Geophys. Res. Oceans 87 (C1), 483–491 (1978–2012).
Hanson, H., Larson, M., Kraus, N.C., 2010. Calculation of beach change under interacting cross-shore and longshore processes. Coast. Eng. 57 (6), 610–619.
Holman, R.A., 1986. Extreme value statistics for wave run-up on a natural beach. Coast. Eng. 9 (6), 527–544.
Hope, M.E., Westerink, J.J., Kennedy, A.B., Kerr, P.C., Dietrich, J.C., Dawson, C., et al., 2013. Hindcast and validation of Hurricane Ike (2008) waves, forerunner, and storm surge. J. Geophys. Res. Oceans 118 (9), 4424–4460.
Hunt, I.A., 1959. Design of seawalls and breakwaters. J. Waterw. Harb. Div. 85, 123–152.
Kennedy, A., Chen, Q., Kirby, J., Dalrymple, R., 2000. Boussinesq modeling of wave transformation, breaking, and runup. I: 1D. J. Waterw. Port Coast. Ocean Eng. 126 (1), 39–47.
Kobayashi, N., Karjadi, E.A., 1994. Surf-similarity parameter for breaking solitary-wave runup. J. Waterw. Port Coast. Ocean Eng. 120 (6), 645–650.
Kobayashi, N., Otta, A., Roy, I., 1987. Wave reflection and run-up on rough slopes. J. Waterw. Port Coast. Ocean Eng. 113 (3), 282–298.
Kraus, N.C., Rosati, J.D., 1997. Interpretation of shoreline-position data for coastal engineering analysis (No. CERC-CETN-II-39) Coastal engineering research center, Vicksburg Ms.
Liu, P.L.F., Cho, Y.S., 1994. Integral equation model for wave propagation with bottom frictions. J. Waterw. Port Coast. Ocean Eng. 120 (6), 594–608.
Lynett, P., 2006. Nearshore wave modeling with high-order Boussinesq-type equations. J. Waterw. Port Coast. Ocean Eng. 132 (5), 348–357.
Lynett, P., Liu, P.L.F., 2005. A numerical study of the run-up generated by three-dimensional landslides. J. Geophys. Res. Oceans 110 (C3) (1978–2012).
Lynett, P., Wu, T., Liu, P., 2002. Modeling wave run-up with depth-integrated equations. Coast. Eng. 46, 89–107.
Lynett, P., Borrero, J., Liu, P.L.-F., Synolakis, C.E., 2003. Field survey and numerical simulations: a review of the 1998 Papua New guinea tsunami. Pure Appl. Geophys. 160, 2119–2146.
Lynett, P., Melby, J., Kim, D.-H., 2010. An application of Boussinesq modeling to hurricane wave overtopping and inundation. Ocean Eng. 37, 135–153.
Madsen, P.A., Fuhrman, D.R., 2008. Run-up of tsunamis and long waves in terms of surf-similarity. Coast. Eng. 55, 209–223.
Madsen, P.A., Schaeffer, H.A., 2010. Analytical solutions for tsunami run-up on a plane beach: single waves, N-waves and transient waves. J. Fluid Mech. 645, 27–57.
Madsen, P.A., Sørensen, O.R., Schäffer, H.A., 1997. Surf zone dynamics simulated by a Boussinesq type model. Part II: Surf beat and swash oscillations for wave groups and irregular waves. Coast. Eng. 32 (4), 289–319.
Mase, H., 1989. Random wave run-up height on gentle slope. J. Waterw. Port Coast. Ocean Eng. 115 (5), 649–661.
Mase, H., Tamada, T., Yasuda, T., Hedges, T.S., Reis, M.T., 2013. Wave runup and overtopping at seawalls built on land and in very shallow water. J. Waterw. Port Coast. Ocean Eng. 139 (5), 346–357.
NDBC, 2014. National Data Buoy Center, National Oceanic and Atmospheric Administration. http://www.ndbc.noaa.gov (Accessed 09/26/2014).
NOAA, 2012. Hurricane Research Division: Atlantic Oceanographic and Meteorological Laboratory Available at: http://www.aoml.noaa.gov/hrd/tcfaq/E11.html.
Park, H., Cox, D.T., Lynett, P.J., Wiebe, D.M., Shin, S., 2013. Tsunami inundation modeling in constructed environments: a physical and numerical comparison of free-surface elevation, velocity, and momentum flux. Coast. Eng. 79, 9–21.
Park, H., Cox, D.T., Petroff, C.M., 2015. An empirical solution for tsunami run-up on compound slopes. Nat. Hazards 76 (3), 1727–1743.
Pullen, T., Allsop, N.W.H., Bruce, T., Kortenhaus, A., Sch, H., Van der Meer, J.W., 2007. Wave overtopping of sea defenses and related structures: assessment manual.
Raubenheimer, B., Guza, R.T., 1996. Observations and predictions of run-up. J. Geophys. Res. Oceans 101 (C11), 25575–25587 (1978–2012).
Romańczyk, W., Boczar-Karakiewicz, B., Bona, J.L., 2005. Extended equilibrium beach profiles. Coast. Eng. 52 (9), 727–744.
Ruggiero, P., Komar, P.D., McDougal, W.G., Marra, J.J., Beach, R.A., 2001. Wave run-up, extreme water levels and the erosion of properties backing beaches. J. Coast. Res. 407–419.
Sallenger Jr., A.H., 2000. Storm impact scale for barrier islands. J. Coast. Res. 890–895.
Saville, T., 1958. Wave run-up on composite slopes. US Beach Erosion Board.
Senechal, N., Coco, G., Bryan, K.R., Holman, R.A., 2011. Wave run-up during extreme storm conditions. J. Geophys. Res. Oceans 116 (C7) (1978–2012).
Stockdon, H.F., Holman, R.A., Howd, P.A., Sallenger, A.H., 2006. Empirical parameterization of setup, swash, and run-up. Coast. Eng. 53 (7), 573–588.
U.S. Army Corps of Engineers (USACE), 1997. Beach and Nearshore Survey Technology. *Coastal Engineering Technical Note*, CETN II-38.
U.S. Army Corps of Engineers (USACE), 2003. Coastal Engineering Manual. Engineer Manual 1110-2-1110p. 2003 (Washington, DC).
Van der Meer, J.W., Stam, C.J.M., 1992. Wave runup on smooth and rock slopes of coastal structures. J. Waterw. Port Coast. Ocean Eng. 118 (5), 534–550.
VanderMeer, J.W., 1998. Wave run-up and overtopping. In: Pilarczyk, K.W. (Ed.), Dikes and Revetments: Design, Maintenance and Safety Assessment. AA Balkema, Rotterdam, The Netherlands, pp. 145–159.
Wang, D.P., Oey, L.Y., 2008. Hindcast of waves and currents in Hurricane Katrina. Bull. Am. Meteorol. Soc. 89 (4), 487–495.

دانشیاری؛ یار دانش پژوهان ایرانی

daneshyari.com